Istraživanja i projektovanja za privredu
ISSN 1451-4117
DOI:10.5937/jaes0-38728
www.engineeringscience.rs

iipp publishing

Journal of Applied Engineering Science
Vol. 20, No. 4, 2022
Original Scientific Paper
Paper number: 20(2022)4, 1016, 1103-1121

EFFECTS OF GEOMETRY AND MATERIAL FACTORS ON THE BEHAVIOR OF STIFFENED OFFSHORE PIPE STRUCTURES UNDER HYDROSTATIC PRESSURE

Ilham Widiyanto[1], Aditya Rio Prabowo[1]*, Teguh Muttaqie[2], Nurul Muhayat[1], Indri Yaningsih[1]*,

Dominicus Danardono Dwi Pria Tjahjana[1], Wibawa Endra Juwana[1], Takahiko Miyazaki[3]

[1] Department of Mechanical Engineering, Universitas Sebelas Maret, Surakarta 57126, Indonesia
[2] Research Center for Hydrodynamics Tech., National Research and Innovation Agency (BRIN), Surabaya 60112, Indonesia
[3] Thermal Energy Conversion System Laboratory, Interdisciplinary Graduate School of Engineering Sciences, Kyushu University, Fukuoka 816-8580, Japan
** aditya@ft.uns.ac.id; indriyaningsih@staff.uns.ac.id*

The world's oil and gas sectors are diverse. They utilize offshore pipes to generate millions of barrels of oil and gas to meet global energy demands. In this study we identified the critical buckling load that occurred on a cylinder shell (also known as radial buckling). Offshore pipe design must meet several criteria, one of which is the requirement for pipes to withstand the external hydrostatic pressure of seawater. The overall buckling load is calculated using the axial compression loading and the pressure on the entire surface of the cylinder shell (radial compression). The finite element analysis (FEA) method is used in our simulation. FEA is run using ABAQUS/CAE software with the Riks algorithm. Different types of cylinder shells are used in the simulation: unstiffened, stringer-stiffened, and ring-stiffened. The cylinder shell is loaded based on the depth of the installation. The material composition of the shell is varied with API 5L X65, copper-nickel alloy, and HY100 steel. The diameter sizes used are 28" (711.2 mm), 30" (762 mm), and 32" (812.8 mm). The simulation results show a critical buckling load for each variation. The critical buckling load is determined by the Young's modulus, geometric length, and moment of inertia. Based on the critical buckling loads generated, we also identify which cylinder shell composition is the strongest.

Keywords: buckling, critical buckling load, cylinder shell, hydrostatic pressure, FEA

1 INTRODUCTION

The global oil and gas industries produce millions of barrels of oil and gas every day. One such producer is Indonesia. Oil and gas are later used as vehicle fuel, aviation turbine fuel, and for many other purposes. Throughout 2018, gas consumption rose due to its increasing contribution to electricity production through geothermal power generators. Based on data from a petroleum company with headquarters in London (BP plc), Indonesia reserved 3.2 billion oil barrels in 2018 (BP's Global Energy Statistics Review 2019). The Indonesian government also launched strategic oil and gas projects, new strategies, and other projects intended to increase oil and gas production. These projects include the Development of the Cricket Mine, Tangguh Train3, Indonesia's Deep Water Development Project, and Inpex's Perpetual Mine Development. Exploration will remain the main focus of SKK Migas in 2021 [1]. SKK Migas will drill 43 exploration wells, conduct 2D Seismic Surveys of 3,569 km, 3D Seismic Surveys of 1,549 km^2, 2D seismic vibrations of 1,000 km, and full tensor gradiometry (FTG) of open areas in the region. Papua is 67,500 km long, and its pseudo-3D seismic open space of 270,000 km makes it one of the longest provinces in the Asia-Pacific region [2]. This will increase the need for offshore pipeline installation to create an oil and gas production channel.

As offshore oil and gas exploitation develops, submarine pipeline design becomes a new challenge for the submarine pipeline industry. Pipe design must meet several criteria, one of which is the requirement for pipes to withstand the external hydrostatic pressure of seawater. The magnitude of the hydrostatic pressure depends on the pipeline installation's depth under the seawater surface. The deeper the structure's position under the seawater surface, the greater the hydrostatic pressure. One significant aspect to consider is the buckling phenomenon of the pipe. In application, the cylinder shell structure is layered and reinforced with the addition of a stiffener for efficiency and to lighten the system [3].

Buckling load is calculated using the axial compression loading, including the pressure on the entire surface of the cylinder shell (radial compression). A cylinder shell must withstand a buckling load, so it is necessary to optimize its strength by considering the situation when it has a light load [4]. One of the methods used for this purpose is adding a stiffener to the cylinder shell. Based on previous studies, there are two types of cylinder shells used in pipeline installation: unstiffened cylinder shells and stiffened cylinder shells. Stiffened cylindrical shells usually use a greater minimum post-buckling force than unstiffened cylindrical shells. This makes stiffened cylinder shells more susceptible to geometric imperfections than unstiffened cylinder shells [5].

There have been several studies regarding buckling in cylinder shells. The testing of subsea pipelines against lateral buckling has been investigated [6]. Subsea pipelines are imperfect sections that are subjected to axial compression loading. In 2019, Zhang et al. [7] examined lateral buckling in pipe structures. Their research involved theoretical and experimental studies using the buckling mechanism's sleeper-snake laying method. A study was also performed

using ABAQUS for experimental tests and numerical analysis, which investigated the effect of loading imperfections on cylinder shells [8]. According to these studies, a stiffener is one way to strengthen the cylindrical shell structure against buckling.

In this study, we comprehensively examine the critical buckling load generated in the cylinder shell, which is due to compression in the radial direction. A critical buckling load is a compressive load under which an object will suddenly buckle. Geometry, material, water depth, and cylinder shell diameter are the parameters used in this study to investigate the critical buckling load in the radial direction (cylinder shell). The geometry uses three types of cylinder shells. The load applied to the cylinder depends on the depth of the water. The load used comprises axial and radial compression. The material in the cylinder shell is considered in this study. Three different types of material are used. The finite element analysis (FEA) method with imperfections is used in our simulation. FEA is run using ABAQUS/CAE software with the Riks algorithm. A convergence mesh is performed with three different sizes. The application of cylinder shells using these parameters could be considered in the case of offshore pipes used for oil and gas distribution under the sea.

2 LITERATURE REVIEW

2.1 Static Risk Analysis

Static risk analysis is used for nonlinear static simulations related to instability. This method involves finding a single equilibrium point in space determined from nodal variables and loading parameters. In ABAQUS, the modification of the algorithm involves changing the distance, which becomes the limit of increasing size (depending on the level of convergence in cases in ABAQUS/Standard) along the tangent to the point of the solution. The formulas for load and displacement using the Riks method are shown in formulas (1) and (2):

$$\text{Load} = \lambda \tilde{P}^N, \tilde{P}^N = P^N / \overline{P} \quad (1)$$

$$\text{Displacement} = \overline{u}^N = (u^N / \overline{u}) \quad (2)$$

where *N* is the degree of freedom of the model, which is the loading pattern defined by one or more loading options on ABAQUS. λ is the magnitude of the load. λP^N is the actual load at any time and u^N is the displacement. Then, we modify the Riks algorithm.

$$\Delta\lambda_0^2(\overline{v}_0^N;1):(\overline{v}_0^N;1) = \Delta l^2 \quad (3)$$

and,

$$\Delta\lambda_0 = \frac{\pm\Delta l}{(\tilde{v}_0^N \tilde{v}_0^N + 1)^{\frac{1}{2}}} \quad (4)$$

$$\Delta\lambda_0(\overline{v}_0^N;1):(\Delta\overline{u}_{-1}^N;\Delta\lambda_{-1}) > 0 \quad (5)$$

then,

$$\Delta\lambda_0(\overline{v}_0^N \Delta\overline{u}_{-1}^N + \Delta\lambda_{-1}) > 0 \quad (6)$$

Based on the level of convergence, l is the specified path length adapted to the ABAQUS/Standard automatic static-load-increasing algorithm. $\bar{v}_0^N$ and $\bar{v}_0^N$ are obtained from the $\bar{u}$ scale. $\Delta\lambda_0$ is the response direction along the tangent line $\Delta\lambda_0(\bar{v}_0^N;1)$. This particular method obtains a positive dot-product in the previous increment $(\Delta\bar{u}_{-1}^N;\ \Delta\lambda_{-1})$. For more details, see ABAQUS=Static User's Manual [9].

2.2 Buckling

Buckling occurs when a shape is not able to preserve its unique form. Buckling is an important geometric problem in which there may be a large deflection that adjusts the structure of the shape [10]. The critical buckling load that can cause instability is calculated via buckling simulations. The characteristic shape due to buckling associated with the structure's response is called the buckling mode shape [11]. Critical buckling load is the load at which an element's or structure's current equilibrium state abruptly shifts from stable to unstable, with or without a substantial response (deformation or deflection). The shorter the object, the higher the critical buckling stress value. In addition, Young's modulus also affects the value of critical buckling stress. The higher the value of Young's modulus, the higher the value of the critical buckling stress. The boundary conditions in a simulation are important, and in general, the buckling load formula is as follows.

$$P_{cr} = \frac{\pi^2 El}{L^2} \quad (7)$$

A nonlinear solver is ideal when modeling structures that do not collapse when buckling. The stiffness matrix in a nonlinear analysis is updated regularly (for each iteration of each load increment) based on the structure's current deformed shape. These calculations are important from a buckling perspective because of the deformation effects before and after buckling. In addition, in many cases, bifurcation instability converts to boundary point instability by introducing small perturbations/imperfections into the system. Real cylinder shells are not straight and often have geometric imperfections affecting their buckling behavior and strength. Early geometric imperfections mean deviations of shells from the 'ideal' geometry. Geometric imperfections can arise in the process of transportation, manufacturing, welding, and fabrication, affecting cylinder shell stability and load-bearing capacity. Determining limit points is the primary goal of nonlinear buckling analysis [12]. The recommended interaction equation for combined axial compression and external pressure is shown in equations (8-10).

$$R_c + R_p = 1 \quad (8)$$

The quantities R_c and R_p denote the compressive and hydrostatic or lateral-pressure load ratios, where R_p is given by

$$R_P = \frac{P}{P_{cr}} \quad (9)$$

P is the applied pressure load and P_{cr} is the allowable pressure load cylinder subjected to external pressure [9].

$$P_{cr} = \frac{0.855}{(1-v^2)^{\frac{3}{4}}} \frac{E\sqrt{\gamma}}{\left(\frac{r}{t}\right)^{\frac{5}{2}}\left(\frac{L}{r}\right)} \quad (10)$$

γ = Correlation (or knockdown) factor

r = Radius cylinder (m)

v = Poisson's ratio

t = Thickness of cylinder (m)

E = Modulus of elasticity (Pa)

L = Cylinder length (m)

2.3 Stiffener

A cylinder shell is one of the typical solutions in offshore pipe design in the submarine pipeline industry. A stiffener is added to increase the critical buckling load's strength. The cylindrical shell model with a stiffener assumes that cylinders are not too heavy, are the same distance apart, and are relatively close [13]. There are two types of stiffeners: the ring-stiffened cylinder shell and the stringer-stiffened cylinder shell. A ring-stiffened cylindrical shell is commonly used in offshore and submersible constructions. High hydrostatic pressure is one consideration in estimating buckling strength for structural safety.

2.4 Material

API 5L X65

API 5L X65 is an economical material and is considered safe for transporting oil and gas. This material combines hardness and strength to support high internal pressures in constructing high-pressure transport pipelines [14]. High-strength low-alloy steel (HSLA) is used as a material for the petroleum industry and has favorable material characteristics [15]. This material has good weldability due to low carbon and alloy elements. At low temperatures this material exhibits toughness and mechanical strength, which are a result of adjusting the chemical composition and manufacturing process in rolling [16]. In addition, API 5L X65 also has high collapse and good corrosion resistance properties for cold-region and deep-water offshore service, increased operating pressure, and reduced size and weight [17].

Copper-Nickel Alloy

Copper-nickel alloys are often found in the offshore pipe industry. These materials have the characteristics of high thermal and electrical conductivity, ease of manufacture, and corrosion resistance [18]. They can resist crevice corrosion and pitting in calm waters. Copper-nickel alloys have been used in various shipbuilding structures for several years, mainly as seawater treatment pipes and heat exchangers, as well as for shipbuilding, offshore, power, and desalination industries.

For pipe diameters >100mm, the copper-nickel 90-10 alloy is considered more sensitive to the phenomenon of imperfection corrosion than the 70-30 copper-nickel alloy. For alloys with less nickel, the seawater velocity is often limited to 3.5 m/s [18]. The addition of nickel can increase the corrosion resistance of the material, high-temperature strength relative to copper, and impact toughness [19].

HY 100 Steel

In 1970, HY100 steel was developed by the US Navy for marine use in pressure vessels, surface ships, and sub-elements. HY 100 steel is a high-performance steel that is often used for critical applications. HY 100 steel is a low-alloy steel often used in applications that require high strength and excellent toughness [20]. In addition, this low-steel alloy is often used in heat exchangers, high-temperature piping, boilers, marine defense, and petrochemical applications. The number "100" in the name of the material denotes its minimum value of yield strength in units of ksi. The elements used to strengthen this material include Cr (1–1.8%), Ni (2.25–3.5%), C (0.2%), and Mo (0.2–0.6%) [21].

2.5 State of the Art

Previous research on cylinder shells has been performed. Table 1 shows the results of studies with different objectives. The dynamic buckling of a composite cylindrical shell under impulsive axial loading was investigated in [22]. Numerical research showed that when the basic geometric imperfection of the body increased, the dynamic load factor (DLF) increased significantly. For short load periods, the dynamic buckling load was close to 14 times larger than the static buckling load for triangular and double-triangular pulse forms. Simultaneously, the dynamic buckling load was four times more than the static load when a trapezoidal pulse form was used. Experimental and computational experiments were used to investigate the buckling behavior of a thin-walled cylindrical shell under localized axial compression pressures [23,24]. There were no differences in the load-bearing capacity, load-displacement curve, or buckling mode. The test results indicate that local axial compressive loads play an important role in the buckling behavior of thin-walled cylinder shells. The critical buckling load of a cylindrical shell rises linearly as the distribution scope of the localized axial load grows within a specific range. The critical buckling load of a cylindrical shell under a uniform axial compression load is similar to that of a cylindrical shell when the distribution scope of localized axial load reaches a specific threshold, such as 150°.

Finite element analysis has been used to analyze the behavior of the complete historical interaction between the outer pipe and the liner and the structural behavior of the lined pipe under axial compression [25]. The presence of the outer pipe avoids or delays the restricted liner's local buckling, which can be increased further by adding internal or external pressures owing to the associated increased interaction stress. Because of the von Mises yield criterion and the tri-axial stress conditions, adding pressure may limit ultimate strength. Experimental testing and the finite element approach have been used to investigate the buckling and strength failure of composite cylindrical shells under hydrostatic pressure [26]. The results indicate that the length-to-radius ratio has no effect on the failure strength pressure; however, the radius–thickness ratio, ply angle, and stacking order significantly affect the critical buckling stress and failure strength stress. A post-buckling analysis of magneto-electro-elastic composite cylindrical shells exposed to multi-field coupled loadings has been undertaken [27]. According to the results, an optimal volume fraction might increase the stability of an MEE composite cylindrical shell under a specific multi-field coupled load. A competitive failure analysis framework for composite laminated cylindrical shells was contrasted under axial compression and torsional loads, as opposed to the prior failure analysis, which only examined buckling failure [28]. The higher the ratios of longitudinal compressive strength to longitudinal modulus, and shear strength to longitudinal modulus, of the composite material, the more possible it is for the material to buckle; otherwise, stress failure occurs. The probability of stress failure increases as the radius-to-thickness ratio decreases. The basic parameters for ring-stiffened cylinders such as shell thickness, stiffener height, stiffener spacing, and overall length of the cylinder can be used to set the failure mode of the structure [10]. The method's accuracy can be improved if the parameters and geometry can be well-defined. Several limitations exist in the proposed ultimate strength formula. It implicitly considers the reduction factors that significantly affect the ultimate strength, such as the residual welding stresses and initial imperfections.

Table 1. Previous buckling research in relation to cylinder shells.

Author	Subject	Target	Conclusion
Zaczynska et al., 2020	Aerospace	AS4/8552 carbon-fiber-reinforced plastic (CFRP)	Numerical research showed that when the basic geometric imperfection of the body increased, the DLF (dynamic load factor) increased significantly. For short load periods, the dynamic buckling load was close to 14 times larger than the static buckling load for triangular and double-triangular pulse forms. Simultaneously, the dynamic buckling load was four times more than the static load when a trapezoidal pulse form was used.

Author	Subject	Target	Conclusion
Jiao et al., 2021	Nuclear	Material steel plates	The critical buckling load of a cylindrical shell rises linearly as the distribution scope of localized axial load grows within a certain range. The critical buckling load of a cylindrical shell under a uniform axial compression load is similar to that of a cylindrical shell when the distribution scope of the localized axial load reaches a specific threshold, such as 150°.
Huy Bich et al., 2013	Nuclear reactors	Ceramic and metal	Internal-ring- and stringer-strengthened shells have the highest critical buckling compression. In a dynamic linear-time load situation, in static analysis, there is no definite point of instability.
Wang et al., 2019	Marine	API 5L X65 and AISI 304L	The presence of the outer pipe avoids or delays the restricted liner's local buckling, which effect can be increased further by adding internal or external pressures owing to the associated increased interaction stress. Because of the von Mises yield criterion and the tri-axial stress conditions, the addition of pressure may limit ultimate strength.
Zhang et al., 2022	Marine	ASTM D3039, ASTM D6641, and ASTM D3518	The results indicate that the length-to-radius ratio had no effect on the failure strength pressure; however, the radius–thickness ratio, ply angle, and stacking order had a significant effect on the critical buckling stress and failure strength stress.
Zhu et al., 2021	Industrial	MEE composite	According to the results, an optimal volume fraction might increase the stability of an MEE composite cylindrical shell under specific multi-field coupled load.
Mahdy et al., 2021	Industrial	Composite	The higher the ratio of longitudinal compressive strength to longitudinal modulus, and shear strength to longitudinal modulus, of the composite material, the more likely it is to buckle; otherwise, stress failure occurs. The probability of stress failure increases as the radius-to-thickness ratio decreases.
Muttaqie et al., 2019	Marine	Steel	The basic parameters of ring-stiffened cylinders such as shell thickness, stiffener height, stiffener spacing, and overall length of the cylinder can be used to set the failure mode of the structure. If the parameters and geometry can be well-defined, then the method's accuracy can be improved. Several limitations exist in the proposed ultimate strength formula. It implicitly considers the reduction factors that significantly affect the ultimate strength, such as the residual welding stresses and initial imperfections.

Research on buckling cylinder shells has been carried out for applications in several fields. Table 1 shows the research carried out with one type of geometry to investigate the buckling phenomenon. Based on the results of the review of the research above, it is concluded that the cylinder shell can be used for offshore pipe modeling either by finite element analysis (FEA) or experimental testing. Offshore pipes are susceptible to the buckling phenomenon,

and parametric studies of this phenomenon are still lacking. In this research, we determine the importance of offshore pipes in the oil and gas industry, and from the results of the above review, we develop a cylindrical shell by varying the geometry and materials used to create a stronger geometry that can withstand critical buckling loads.

3 BENCHMARKING ANALYSIS

Theoretical and analytical studies have investigated unstiffened cylindrical shells at external pressure [29]. Six-cylinder shells with a material thickness of t =1 mm made of 304 stainless steel were used in our experiments. Shell cover thickness was t_1 = 10 mm and diameter was D_1 = 120 mm for both lower- and upper-cylinder shell bodies. The utilized cylinder (l) has a length of 49.67 mm. The cylinder body is ten times thinner than the top and bottom caps. Table 1 shows the sample diameter, medium length, and standard deviation. According to our research, all actual cylinders have a thickness (t) of 1 mm and a diameter (D) of 100 mm. The percentage of poisson's ratio (v) that was applied was 0.25. Fig. 1 shows the measurements of the model's dimensions.

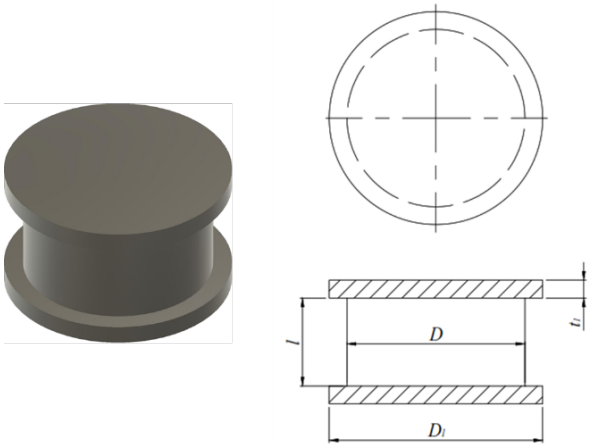

Fig. 1. Measurement specimen dimensions.

The experimental results were compared to the theoretical analysis utilizing the approaches commonly used to develop the cylinder pressure hull of the deep-diving manned submersibles CCS2013 and ABS2012. The obtained results were then compared to the FEM using ABAQUS/CAE software. In this study, the mesh size was 2.5 mm. Five eigenmodes were used in the simulation. A nonlinear simulation was run using the first eigenmode. In respect of nonlinear buckling, the Riks method was used. The imperfection used was 0.2 times the thickness of the model. Table 2 shows the dimensional data for all of the investigated specimens, and this study's first variation of the resulting data was used. As for the simulation step settings, arc length incrementation was conducted in this study. In the specimen dimension table, LR denotes the ratio of length and radius. Table 3 shows the input of arc-length increment.

Table 2. Measured data dimensions for all tested specimens [29].

	D_{max} (mm)	D_{min} (mm)	D_{ave} (mm)	D_{std} (mm)	l_{ave} (mm)	l_{std} ($\times 10^{-3}$) (mm)	D_{ave}/t_{ave} (mm)	l_{ave}/D_{ave} (mm)
LR1.0	**101.73**	**101.46**	**101.60**	**0.135**	**49.67**	**6.22**	**111.40**	**0.49**
LR1.5	101.77	101.36	101.58	0.205	75.70	6.46	111.14	0.75
LR2.0	101.82	101.35	101.60	0.235	98.82	6.94	110.68	0.97

Table 3. Arc length increment [29].

Parameters	Unit	Value
Initial arc length	mm	0.1
Minimum arc length	mm	0.00001
Maximum arc length	mm	0.5
Number of iterations	-	100

Based on the results of a previous study [29], yield stress σ_{yp} = 323.18 MPa and Young's modulus E = 176.05 GPa are the material properties of 304 stainless steel. It was assumed that the material was elastic-perfectly plastic. The experimental conditions of the cylindrical shell were as follows: one end of the cylindrical shell was fixed, while the other end was fastened such that only axial movement was permitted. In the finite element analysis (FEA), an external pressure of 1 MPa was applied to the entire area of the cylindrical shell (radial compression). Experiments were carried out to determine the values of material properties. According to a theoretical study, the buckling load calculation result for CCS2013 is 4.50 MPa and for ABS2012 it is 3.60 MPa. Fig. 2 shows the comparison of the nonlinear buckling simulation and experimental results from [29]. In their experiment, the critical buckling load was

4.56 MPa. It was 4.17 MPa according to the nonlinear buckling simulation result with FE analysis. When these values were estimated using Equations (8) to (10), the design formula value produced was 4.14 MPa. Table 4 shows the critical buckling load data. Thus, the FEA method is considered valid for carrying out the research.

Table 4. Critical buckling load results [29].

Methods	Value (MPa)
Experiment	4.56
Finite element analysis	4.17
Design formula	4.14

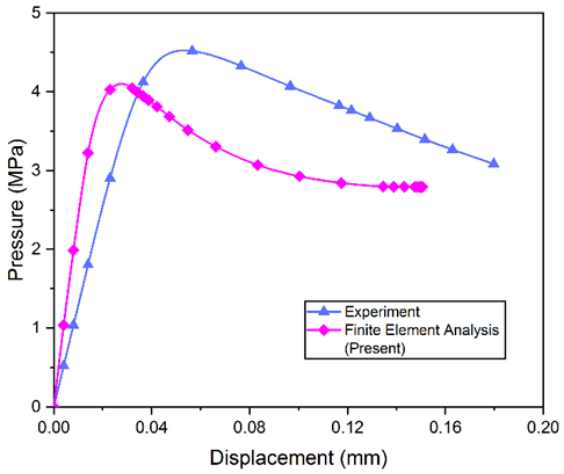

Fig. 2. Comparison of experimental and simulated critical buckling loads for LR 1.0 cylindrical shell.

4 METHODOLOGY

4.1 Geometrical design

In this study we used a cylinder shell design. Three types of cylinder shell geometries can be used: unstiffened, stringer-stiffened, and ring-stiffened cylinder shell. Each geometry has the same structural weight, but the thicknesses are different in each type. The width of the stiffener used is w = 90 mm. The cylinder shell thickness can be seen in Table 5. The cylinder shell (l) length in those three types is 2000 mm. The top and bottom of the cylinder shell have shell caps. Shell caps are ten times the thickness of the cylinder shell. Each model has four stiffeners. The stringer-stiffened cylinder shell is installed along the length of the cylinder shell. The ring-stiffened cylinder shell is installed at a distance of (l_1) 400 mm. The cylinder shell design can be seen in Fig. 3.

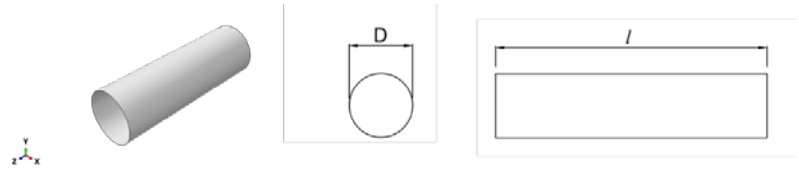

Fig. 3. Geometrical cylindrical shell: (a) unstiffened cylinder shell

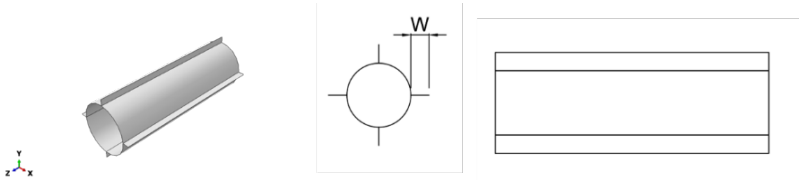

Fig. 3. Geometrical cylindrical shell: (b) stringer-stiffened cylinder shell

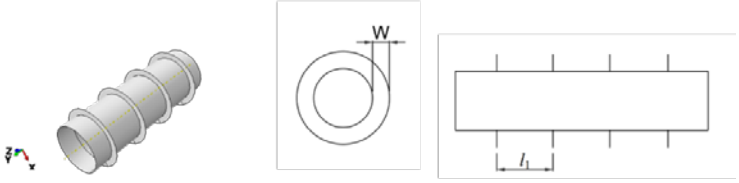

Fig. 3. Geometrical cylindrical shell: (c) ring-stiffened cylinder shell.

Table 5. Thickness of cylinder shells.

Model	Thickness (mm)	Model	Thickness (mm)	Model	Thickness (mm)
S1-1-A	4.2760	S1-2-A	3.9910	S1-3-A	3.7415
S1-1-B	3.7716	S1-2-B	3.5202	S1-3-B	3.3001
S1-1-C	4.2760	S1-2-C	3.9910	S1-3-C	3.7415
S2-1-A	3.9249	S2-2-A	3.6000	S2-3-A	3.3250
S2-1-B	3.4617	S2-2-B	3.1754	S2-3-B	2.9327
S2-1-C	3.9249	S2-2-C	3.6000	S2-3-C	3.3250
S3-1-A	3.8628	S3-2-A	3.4975	S3-3-A	3.1824
S3-1-B	3.4070	S3-2-B	3.0850	S3-3-B	2.8069
S3-1-C	3.8628	S3-2-C	3.4975	S3-3-C	3.1824

4.2 Material properties

In this study, the meshing of the cylindrical shell was also simulated using the FEA method. The software used was ABAQUS/CAE. Three types of materials were used: API 5L X65, copper-nickel alloy, and HY100 steel. Material selection was based on the materials often used in the gas and oil exploration industry. API 5L X65 steel welded pipe with standards EN 10204 3.1 was used. Copper-nickel alloy material based on the Unified Numbering System (UNS) standard C70600 was used. HY100 steel based on specification MIL-S-21952 T9074-BD-GIB-010/0300 was used. The materials were assumed to be elastic-perfectly plastic materials. The materials were used to simulate the similar behavior of the outer pipe. Material properties can be seen in Table 6.

Table 6. Material properties.

Parameter	API 5L X65	Copper-Nickel Alloy	HY100 Steel
Mass density (kg/mm^3)	7.85 x 10^{-6}	8.90 x 10^{-6}	7.85 x 10^{-6}
Modulus of elasticity (MPa)	211,330	140,000	207,000
Yield stress (MPa)	552	372.316	784
Poisson's ratio (-)	0.3	0.34	0.3

4.3 Finite Element Analysis

4.3.1 Mesh convergence

Meshing involves dividing the component to be analyzed into small or discrete elements. The higher the level of convergence, the smaller the mesh used. In this study we performed mesh convergence with three mesh sizes; namely, 25 mm, 75 mm, and 125 mm. The three meshes were tested with a cylindrical shell geometry without stiffeners for each diameter size. S4R (4-node quadrilateral finite membrane strain linear reduction integrated shell) was used as the meshing element. The meshing model can be seen in Fig. 4. The simulation results show that meshing with a size of 25 mm resulted in convergence. For a smaller mesh size, there was no difference in value. The results of the mesh convergence can be seen in Table 7.

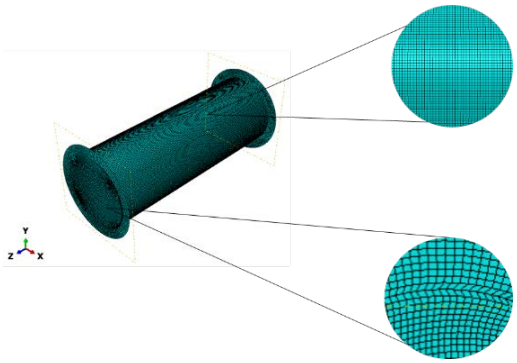

Fig. 4. Mesh modeling.

Table 7. Critical buckling load from mesh convergence simulations.

Model	Mesh size (mm)	Critical buckling load (MPa)
S1-1-A	25	0.682
	75	0.684
	125	0.685
S2-1-A	25	0.561
	75	0.565
	125	0.566
S3-1-A	25	1.664
	75	1.803
	125	2.210

4.3.2 Boundary Conditions

In this study, the applied load was in the form of hydrostatic pressure. Hydrostatic pressure is uniform external pressure throughout the cylindrical shell area (radial compression). Meanwhile, axial compression was applied to one end of the cylinder shell. The load was given for three different depths. The value of the hydrostatic pressure depends on the depth. The depth can be estimated using the density of seawater. The three depths of seawater were 250 m, 500 m, and 750 m below sea level. The boundary conditions of the cylinder shell were as follows: at one end was completely fixed; the other end allowed only axial movement. The result of linear compression is the eigenvalue. The first eigenmode value was used as a load to simulate nonlinear buckling. The boundary condition model can be seen in Fig. 5.

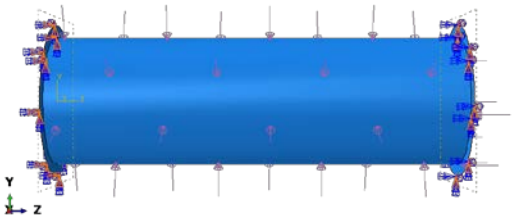

Fig. 5. Boundary condition model.

In the nonlinear simulation, the step module uses the Riks algorithm. The Riks algorithm parameters can be seen in Table 8. This simulation applies NLGEOM (nonlinear geometry) in ABAQUS/CAE software. Geometry imperfection is considered in this simulation. The imperfection used is 0.2 thickness of the cylinder shell. The results obtained are expressed in terms of the load proportionality factor (LPF). LPF is used to determine the critical buckling load value. The arc length is used to calculate displacement. Equations (11) and (12) can be used to calculate the critical buckling load and displacement values in post-processing.

$$P = LPF.P_0 \quad (11)$$

$$S = \theta.R \quad (12)$$

where P is the critical buckling load, P_0 is the initial load input, S is the arc length, R is the radius of the cylinder shell, and θ is the displacement of the shell cylinder.

Table 8. Parameter arc length.

Parameter	Unit	Value
Arc length	mm	0.01
Minimum arc length	mm	1×10^{-10}
Maximum arc length	mm	1×10^{36}
Number of iterations	-	100

4.4 Study Variation

In this study, there are four variations; namely, geometry, diameter, depth, and material. The geometric distribution is an unstiffened cylinder shell (S1), stringer-stiffened cylinder shell (S2), and ring-stiffened cylinder shell (S3). Variations in diameter are symbolized by 711.2 mm (1), 762 mm (2), and 812.8 mm (3). The load variations are indicated by 250 m (α), 500 m (β), and 750 m (γ). The material variation is API 5L X65 (A), copper-nickel alloy (B), and HY100 steel (C).

5 CALCULATION RESULTS AND DISCUSSION

5.1 Critical Buckling Load

The buckling simulation results for each model are discussed in this section. The critical buckling load values are variable for each model. Simulations were run based on the results of various studies. The geometric model was used to sort the simulation results. The results shown are in respect of the FEA from the simulation and are compared with the design formula. The simulation results for a cylinder shell diameter of 711.2 mm are shown in Table 9. Table 10 shows simulation findings for a diameter of 762 mm, whereas Table 11 shows buckling simulation results for a diameter of 812.8 mm.

Table 9. Simulation results for cylinder shell diameter of 711.2 mm.

Model	Finite Element Analysis Critical Buckling Load (MPa)	Design Formula Critical Buckling Load (MPa)
S1-1-α-A	0.682	0.676
S1-1-α-B	0.346	0.344
S1-1-α-C	0.668	0.663
S1-1-β-A	0.684	0.679
S1-1-β-B	0.346	0.344
S1-1-β-C	0.670	0.665
S1-1-γ-A	0.684	0.679
S1-1-γ-B	0.346	0.344
S1-1-γ-C	0.670	0.665
S2-1-α-A	0.561	0.546
S2-1-α-B	0.287	0.279
S2-1-α-C	0.550	0.535
S2-1-β-A	0.563	0.548
S2-1-β-B	0.288	0.280
S2-1-β-C	0.552	0.537
S2-1-γ-A	0.563	0.548
S2-1-γ-B	0.287	0.280
S2-1-γ-C	0.549	0.534
S3-1-α-A	1.664	1.638
S3-1-α-B	0.838	0.825
S3-1-α-C	1.725	1.698
S3-1-β-A	1.664	1.638
S3-1-β-B	0.839	0.825
S3-1-β-C	1.725	1.697
S3-1-γ-A	1.665	1.638
S3-1-γ-B	0.839	0.825
S3-1-γ-C	1.724	1.697

Model	Finite Element Analysis Critical Buckling Load (MPa)	Design Formula Critical Buckling Load (MPa)
Variation Coeff. (%)	0.621	0.622

Table 10. Simulation results for cylinder shell diameter of 762 mm.

Model	Finite Element Analysis Critical Buckling Load (MPa)	Design Formula Critical Buckling Load (MPa)
S1-2-α-A	0.555	0.551
S1-2-α-B	0.273	0.271
S1-2-α-C	0.554	0.550
S1-2-β-A	0.555	0.551
S1-2-β-B	0.269	0.267
S1-2-β-C	0.555	0.551
S1-2-γ-A	0.562	0.558
S1-2-γ-B	0.260	0.258
S1-2-γ-C	0.555	0.551
S2-2-α-A	0.450	0.438
S2-2-α-B	0.235	0.228
S2-2-α-C	0.440	0.429
S2-2-β-A	0.451	0.439
S2-2-β-B	0.234	0.227
S2-2-β-C	0.442	0.430
S2-2-γ-A	0.451	0.439
S2-2-γ-B	0.233	0.227
S2-2-γ-C	0.442	0.430
S3-2-α-A	1.186	1.167
S3-2-α-B	0.611	0.601
S3-2-α-C	1.197	1.178
S3-2-β-A	1.149	1.131
S3-2-β-B	0.607	0.597
S3-2-β-C	1.181	1.163
S3-2-γ-A	1.154	1.135
S3-2-γ-B	0.605	0.596
S3-2-γ-C	1.178	1.160
Variation Coeff. (%)	0.546	0.547

Table 11. Simulation results for cylinder shell diameter of 812.8 mm.

Model	Finite Element Analysis Critical Buckling Load (MPa)	Design Formula Critical Buckling Load (MPa)
S1-3-α-A	0.411	0.408
S1-3-α-B	0.201	0.199
S1-3-α-C	0.405	0.402
S1-3-β-A	0.408	0.405

Model	Finite Element Analysis Critical Buckling Load (MPa)	Design Formula Critical Buckling Load (MPa)
S1-3-β-B	0.200	0.198
S1-3-β-C	0.400	0.397
S1-3-γ-A	0.408	0.405
S1-3-γ-B	0.200	0.198
S1-3-γ-C	0.400	0.397
S2-3-α-A	0.359	0.350
S2-3-α-B	0.179	0.174
S2-3-α-C	0.353	0.344
S2-3-β-A	0.361	0.351
S2-3-β-B	0.182	0.177
S2-3-β-C	0.353	0.344
S2-3-γ-A	0.361	0.351
S2-3-γ-B	0.182	0.177
S2-3-γ-C	0.353	0.344
S3-3-α-A	0.869	0.855
S3-3-α-B	0.435	0.428
S3-3-α-C	0.909	0.895
S3-3-β-A	0.849	0.836
S3-3-β-B	0.435	0.428
S3-3-β-C	0.855	0.841
S3-3-γ-A	0.850	0.836
S3-3-γ-B	0.434	0.427
0S3-3-γ-C	0.857	0.843
Variation Coeff. (%)	0.531	0.532

Each geometric model was investigated with water depth. Fig. 6 shows the simulation results for the unstiffened cylinder shell model for variations in water depth. The highest critical buckling load in the S1-1-β-A model is 0.684 MPa, according to these data. Meanwhile, the lowest critical buckling load is S1-3-γ-B, with 0.2 MPa.

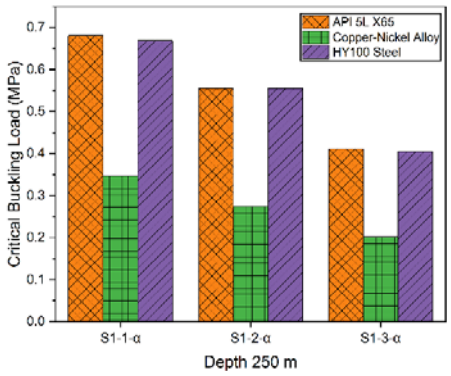

(a)

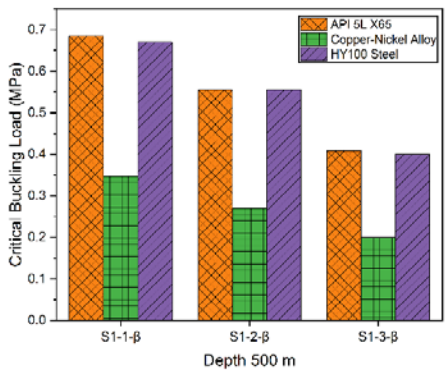

(b)

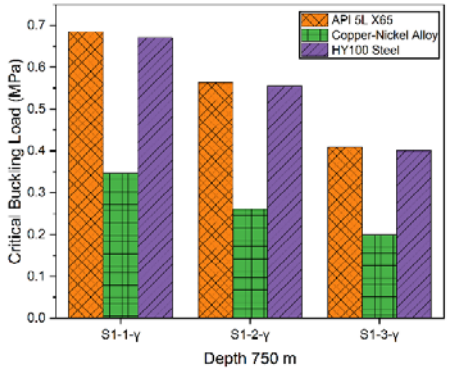

(c)

Fig. 6. Simulation results for unstiffened cylinder shell geometry with water depth: (a) 250 m, (b) 500 m, (c) 750 m.

The simulation results for the stringer-stiffened cylinder shell (S2) geometry for variations in water depth can be seen in Fig. 7. The S2-1-β-A model has the highest critical buckling load value of 0.563 MPa. The lowest essential weight of buckling load in the S2-3-α-B model is 0.179 MPa.

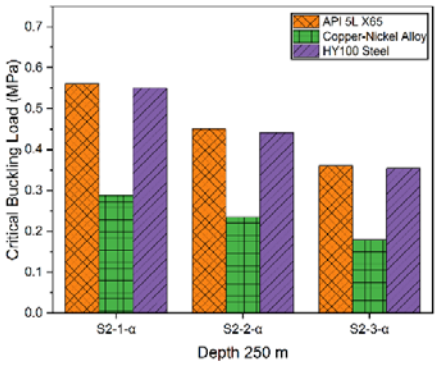

(a)

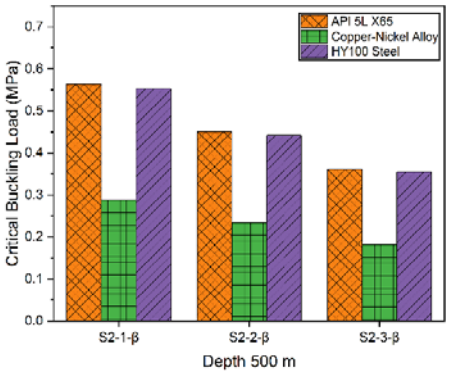

(b)

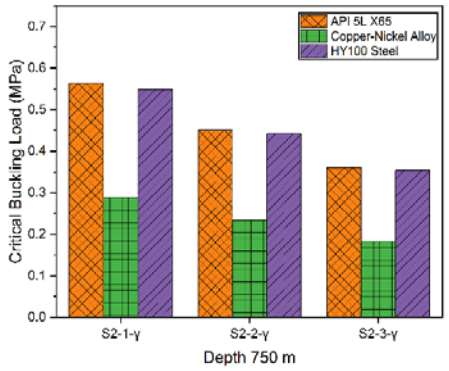

(c)

Fig. 7. Results for stringer-stiffened cylinder shell geometry simulation against water depth: (a) 250 m, (b) 500 m, (c) 750 m.

Fig. 8 shows the simulation results for variations in water depth on the ring-stiffened cylinder shell (S3). The S3-1-β-C model has the highest critical buckling load value of 1.725 MPa. For the S3-3-γ-B model, the lowest critical buckling load is 0.434 MPa.

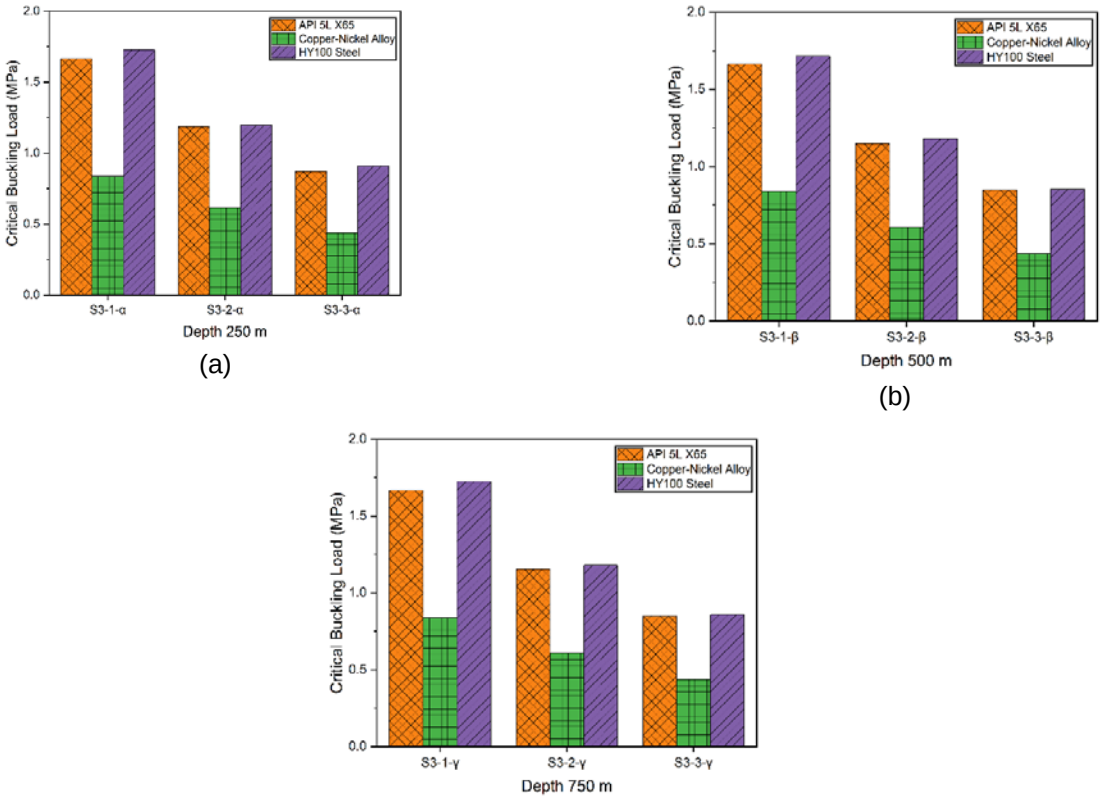

Fig. 8. Simulation results for ring-stiffened cylinder shell (S3) geometry with water depth: (a) 250 m, (b) 500 m, (c) 750 m.

In the geometry of the cylindrical shell without stiffeners (S1) for water depth, the highest critical buckling load value is found at a depth of 500 m with the API 5L X65 material with a diameter of 711.2 mm. The yield stress on a material can determine the critical buckling load value. This also applies to the geometry of the stringer-stiffened cylinder shell (S2). Geometry with API 5L X65 steel material with a diameter of 711.2 mm at a depth of 500 m produces the highest critical buckling load value. However, this result is different from that obtained for the ring-stiffened cylinder shell (S3). In this geometry, the highest critical buckling load experienced on HY100 steel material with a diameter of 711.2 at a depth of 250 m has significant results. Based on the geometric variation, the ring-stiffened cylinder shell produces the highest critical buckling load compared to the others, while the material variation for API 5L X65 is suitable for use in unstiffened and stringer-stiffened cylinder shells. However, the ring-stiffened cylinder shell geometry using HY100 steel material produces the highest critical buckling load. We found that the cylindrical shell with a ring stiffener has a high critical buckling load compared to other geometries. In terms of material, for a deeper installation, the critical buckling load decreases [30].

5.2 Displacement

In this study, the output is obtained in the form of displacement. ABAQUS/CAE software can also determine the displacement of a simulated model. The variation in this study was used to find the displacement value for each model. In the diameter variation of 711.2 mm, the highest displacement was found in the S2-1-γ-A model with a value of 184.5 mm, and the lowest occurred in the S3-1-β-B model with a result of 16.56 mm. The displacement diameter of 711.2 mm can be seen in Fig. 9. At a diameter of 762 mm, the highest displacement was found in the S2-2-β-A model with a value of 151.9 mm, and the lowest was found in the S3-2-α-C model with a result of 14.94 mm. The displacement diameter of 762 mm can be seen in Fig. 10. At a diameter of 812.8 mm, the highest value was found in the S1-3-β-C model with 140.7 mm. At the same time, the lowest value was found in the S3-3-β-B model with a value of 13.09 mm. The results of the displacement diameter of 812.8 mm can be seen in Fig. 11. The simulation results generally found that for larger diameter and depth values, the load on the cylinder shell will decrease the displacement value. The type of geometry also affects the displacement value. A ring-stiffener was added and proven to reduce the displacement value.

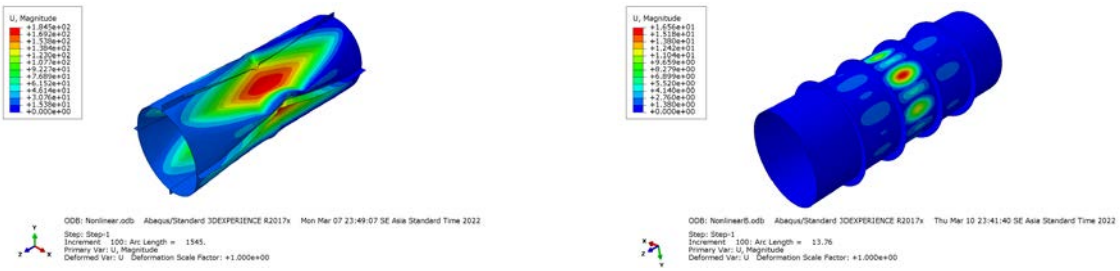

(a) (b)

Fig. 9. Displacement results for diameter of 711.2 mm: (a) S2-1-γ-A, (b) S3-1-β-B.

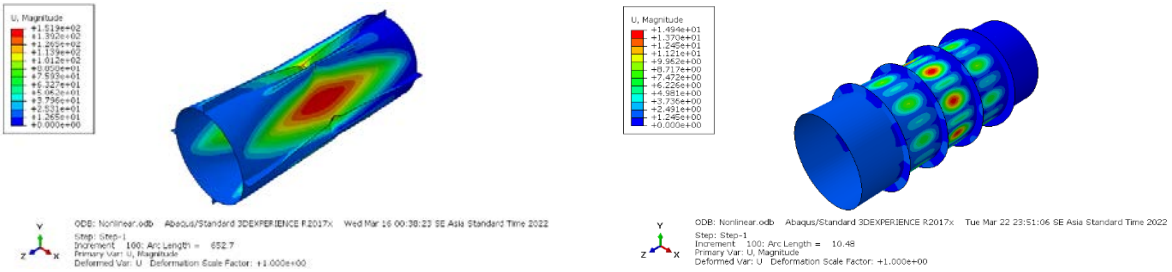

(a) (b)

Fig. 10. Displacement results for diameter of 762 mm: (a) S2-2-β-A, (b) S3-2-α-C.

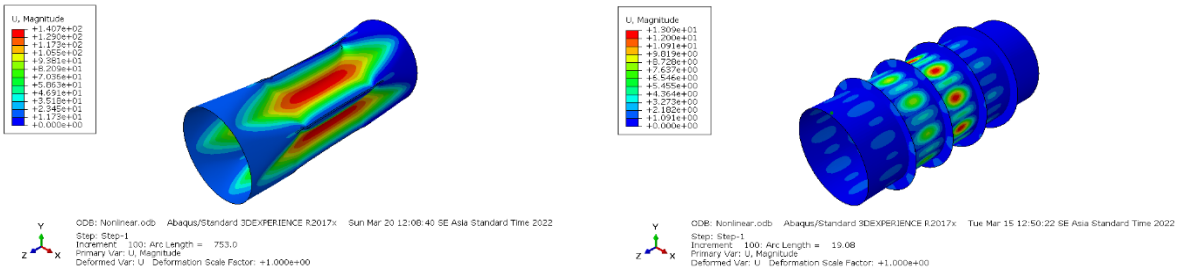

(a) (b)

Fig. 11. Displacement results for diameter of 812.8 mm: (a) S1-3-β-C, (b) S3-3-β-B.

5.3 Von Mises Stress

After performing the buckling simulation, the result is von Mises stress [31–35]. The results show that the cylinder shell with the ring stiffener experienced better stress. The distribution of blue and green colors is more dominant, so they do not experience significant stress. The red contour is the part of the cylinder shell that experiences the highest stress. Fig. 12 shows the von Mises graph in each increment. In this study, we used default incrementation settings in ABAQUS. Incrementation is the time step size that occurs during the simulation process. In this particular case, each increment defines the von Mises stress value in the cylinder shell. The increments used were 5, 10, and 15. In increments of 15, the S3-1-α-A model experienced the highest stress, 552 MPa. The smallest stress was in the S1-1-α-A model of 0.4254 MPa in 5 increments. The contours of the color distribution can be seen in Fig. 13-15. After reaching the yield stress point, the ring-stiffened cylinder shell geometry still shows blue and green contours.

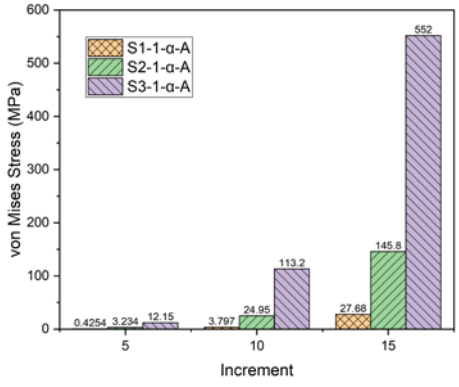

Fig. 12. Graph of von Mises stress increment in buckling simulation.

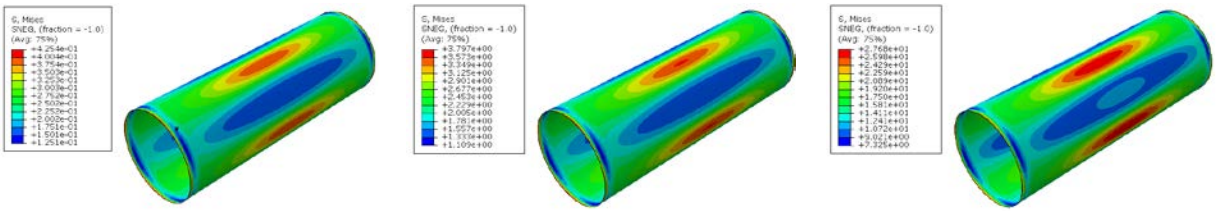

(a) (b) (c)

Fig. 13. The contours of von Mises stress on the S1-1-α-A model at each increment: (a) 5, (b) 10, (c) 15.

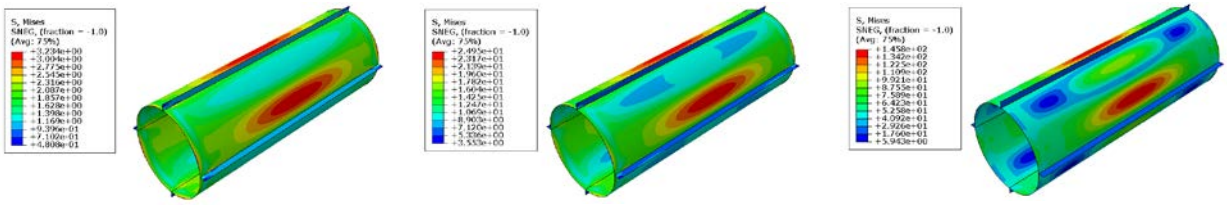

(a) (b) (c)

Fig. 14. The contours of von Mises stress on the S2-1-α-A model at each increment: (a) 5, (b) 10, (c) 15.

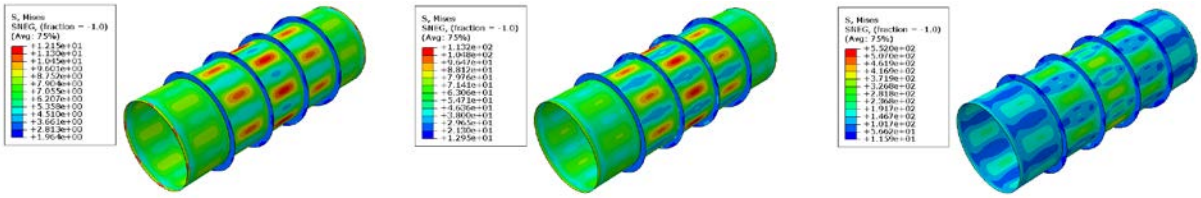

(a) (b) (c)

Fig. 15. The contours of von Mises stress on the S3-1-α-A model at each increment: (a) 5, (b) 10, (c) 15.

5.4 Strain

Based on the simulation, the strain [36–40] on the model was obtained. The plastic strain contour shows that the ring-stiffened cylinder shell experiences better strain than the unstiffened and stringer-stiffened cylinder shells. This is evidenced by the distribution of blue and green colors, which do not indicate significant strain. From the graph in Fig. 16, the treatment of plastic strains on the geometry variation is subject to the same dimensions, depth, and material. These results prove that the unstiffened cylinder shell produces the highest strain value compared to the ring-stiffened cylinder shell. The higher the strain value, the easier it will be for the cylinder shell to elongate. The PEEQ value of the plastic strain in the unstiffened cylinder shell reached 0.5887. The stringer-stiffened cylinder shell produced a strain value of 0.2798. The significant difference was in the ring-stiffened cylinder shell, which had a value of 0.0663. Fig. 17 shows the distribution of PEEQ plastic strain after buckling simulation.

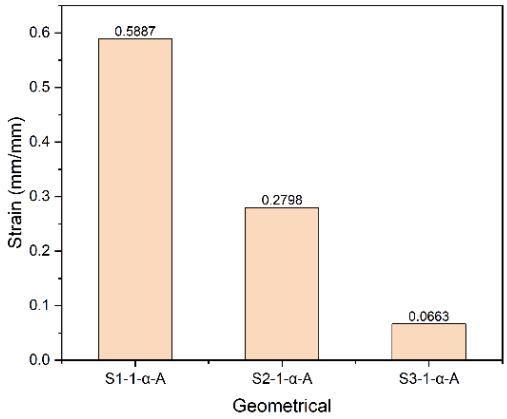

Fig. 16. PEEQ strain graphs for cylinder shell geometry.

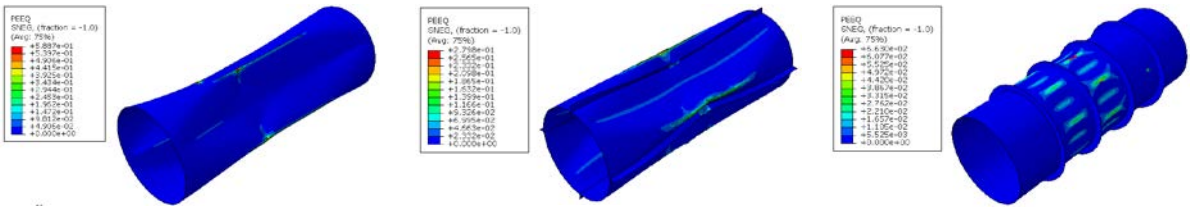

(a) (b) (c)

Fig. 17. PEEQ strain contours on cylinder shell geometry: (a) S1-1-α-A, (b) S2-1-α-A, (c) S3-1-α-A.

6 CONCLUSIONS AND FUTURE WORK

An offshore pipe is a vital component used for the distribution of oil and gas. Our research was conducted with a cylinder shell used as a simulation model. This cylinder shell was varied in terms of stiffeners, dimensions, loads from each depth, and materials. From the simulation results, the following can be concluded:

- The design formula and FEA calculations are not significantly different, so the method applied follows the procedure.
- The addition of a stiffener can increase the critical buckling load. The ring-stiffened cylinder shell produces a high critical buckling load compared to the unstiffened and stringer-stiffened cylinder shells.
- The critical buckling load value is affected by diameter variation. The thicknesses used in this study were different since it was assumed that the model used had the same load. The value of the critical buckling load decreases as the diameter increases.
- Various installation depths have an impact on critical buckling load results. The deeper the installation location, the higher the load in the form of pressure on the cylinder shell. This will make the critical buckling load decrease.
- The material applied to the cylinder shell also affects the critical buckling load value. A cylinder shell made with API 5L X65 material is more suitable for unstiffened and stringer-stiffened types. In comparison, the HY100 steel material may be used on the ring-stiffened cylinder shell. The critical buckling load for the ring-stiffened cylinder shell is therefore higher than for other materials.
- Output displacement appears in this simulation. The larger the diameter and depth of the model, the larger the resulting displacement will be. The addition of a ring-stiffener can reduce the displacement significantly.
- When compared to the unstiffened cylinder shell and stringer-stiffened cylinder shell, the ring-stiffened cylinder shell generates higher von Mises stress and strain after buckling simulation.
- This invention can be used as a reference in the offshore pipeline industry. The research results can be adapted to market needs, environmental conditions, and cost considerations in the manufacturing process for making offshore pipes.

We found that adding a ring-stiffener can increase the critical buckling load. In addition, the ring-stiffener can reduce the displacement of the given load. This study can help predict and overcome the excessive buckling of offshore pipes. However, our FEA results must be tested by experimental analysis to obtain more accurate findings. Additionally, investigations related to this research will continue to be developed to obtain significant results.

7 ACKNOWLEDGMENTS

This research was funded by Universitas Sebelas Maret under funding scheme Kolaborasi Internasional (KI-UNS) with contract/grant number 254/UN27.22/PT.01.03/2022. The grant is gratefully acknowledged by authors.

8 REFERENCES

[1] SKK Migas, 2020 Annual Report: Towards 1 Million BOPD & 12 BSCFD in 2030, SKK Migas. (2020).

[2] PwC, Oil and Gas in Indonesia. Taxation Guide, (2019).

[3] J. Liu, B. Yu, Y. Zhou, Y. Zhang, M. Duan, The buckling of spherical-cylindrical composite shells by external pressure, Compos. Struct. 265 (2021). https://doi.org/10.1016/j.compstruct.2021.113773.

[4] B. Wang, M. Yang, D. Zhang, D. Liu, S. Feng, P. Hao, Alternative approach for imperfection-tolerant design optimization of stiffened cylindrical shells via energy barrier method, Thin-Walled Struct. 172 (2022) 108838. https://doi.org/10.1016/j.tws.2021.108838.

[5] H.S. Shen, Postbuckling behavior of plates and shells, 2017. https://doi.org/10.1142/10208.

[6] I. Guha, D.J. White, M.F. Randolph, Parametric solution of lateral buckling of submarine pipelines, Appl. Ocean Res. 98 (2020) 102077. https://doi.org/10.1016/j.apor.2020.102077.

[7] Z. Zhang, J. Yu, H. Liu, Z. Chen, Experimental and finite element study on lateral global buckling of pipe-in-pipe structure by active control method, Appl. Ocean Res. 92 (2019) 101917. https://doi.org/10.1016/j.apor.2019.101917.

[8] H.N.R. Wagner, C. Hühne, M. Janssen, Buckling of cylindrical shells under axial compression with loading imperfections: An experimental and numerical campaign on low knockdown factors, Thin-Walled Struct. 151 (2020) 106764. https://doi.org/10.1016/j.tws.2020.106764.

[9] R.J. Boulbes, Troubleshooting Finite-Element Modeling with Abaqus: With Application in Structural Engineering Analysis, 2020. https://doi.org/https://doi.org/10.1007/978-3-030-26740-7_2.

[10] T. Muttaqie, D.Q. Thang, A.R. Prabowo, S.R. Cho, J.M. Sohn, Numerical studies of the failure modes of ring-stiffened cylinders under hydrostatic pressure, Struct. Eng. Mech. 70 (2019) 431–443. https://doi.org/10.12989/sem.2019.70.4.431.

[11] H.M. Lee, G.H. Yoon, Size optimization method for controlling the buckling mode shape and critical buckling temperature of composite structures, Compos. Struct. 255 (2021) 112902. https://doi.org/10.1016/j.compstruct.2020.112902.

[12] K. Liang, P. Hao, B. Wang, Q. Sun, A novel reduced-order modeling method for nonlinear buckling analysis and optimization of geometrically imperfect cylinders, Int. J. Numer. Methods Eng. 122 (2021) 1456–1475. https://doi.org/10.1002/nme.6585.

[13] R. Wei, K. Shen, G. Pan, Optimal design of trapezoid stiffeners of composite cylindrical shells subjected to hydrostatic pressure, Thin-Walled Struct. 166 (2021) 108002. https://doi.org/10.1016/j.tws.2021.108002.

[14] M.C. De Oliveira, R.M. Figueredo, H.A. Acciari, E.N. Codaro, Corrosion behavior of API 5L X65 steel subject to plastic deformation, J. Mater. Res. Technol. 7 (2018) 314–318. https://doi.org/10.1016/j.jmrt.2018.02.006.

[15] Z. Gao, B. Gong, Q. Xu, D. Wang, C. Deng, Y. Yu, High cycle fatigue behaviors of API X65 pipeline steel welded joints in air and H2S solution environment, Int. J. Hydrogen Energy. 46 (2021) 10423–10437. https://doi.org/10.1016/j.ijhydene.2020.12.140.

[16] D.T. Buzzatti, L.F. Kanan, G. Dalpiaz, A. Scheid, C.E. Fortis Kwietniewski, Effect of heat input and heat treatment on the microstructure and toughness of pipeline girth friction welded API 5L X65 steel, Mater. Sci. Eng. A. 833 (2022) 142588. https://doi.org/10.1016/j.msea.2021.142588.

[17] V.S. Liduino, M.T.S. Lutterbach, E.F.C. Sérvulo, Corrosion behavior of carbon steel API 5L X65 exposed to seawater, Int. J. Eng. Tech. Res. 7 (2017) 70–74.

[18] Z. Tan, T. Ma, L. Zhang, W. Zhang, R. Jia, D. Cao, H. Ji, Relationship between corrosion resistance and microstructure of copper-nickel alloy pipes in marine engineering, Mater. Sci. Forum. 944 MSF (2018) 389–397. https://doi.org/10.4028/www.scientific.net/MSF.944.389.

[19] T. Yonezawa, Nickel-Based Alloys, 2020. https://doi.org/10.1016/B978-0-12-803581-8.00676-7.

[20] M. Imran, D. Shi, L. Tong, H.M. Waqas, Design optimization of composite submerged cylindrical pressure hull using genetic algorithm and finite element analysis, Ocean Eng. 190 (2019) 106443. https://doi.org/10.1016/j.oceaneng.2019.106443.

[21] J.J.S. Dilip, G.D.J. Ram, T.L. Starr, B. Stucker, Selective laser melting of HY100 steel: Process parameters, microstructure and mechanical properties, Addit. Manuf. 13 (2017) 49–60. https://doi.org/10.1016/j.addma.2016.11.003.

[22] M. Zaczynska, H. Abramovich, C. Bisagni, Parametric studies on the dynamic buckling phenomenon of a composite cylindrical shell under impulsive axial compression, J. Sound Vib. 482 (2020) 115462. https://doi.org/10.1016/j.jsv.2020.115462.

[23] P. Jiao, Z. Chen, H. Ma, P. Ge, Y. Gu, H. Miao, Thin-Walled Structures Buckling behaviors of thin-walled cylindrical shells under localized axial compression loads , Part 1 : Experimental study, 166 (2021). https://doi.org/10.1016/j.tws.2021.108118.

[24] P. Jiao, Z. Chen, H. Ma, P. Ge, Y. Gu, H. Miao, Thin-Walled Structures Buckling behaviors of thin-walled cylindrical shells under localized axial compression loads , Part 2 : Numerical study, 169 (2021). https://doi.org/10.1016/j.tws.2021.108330.

[25] F.C. Wang, W. Li, L.H. Han, Interaction behavior between outer pipe and liner within offshore lined pipeline under axial compression, Ocean Eng. 175 (2019) 103–112. https://doi.org/10.1016/j.oceaneng.2019.02.025.

[26] X. Zhang, Z. Li, P. Wang, G. Pan, Experimental and numerical analyses on buckling and strength failure of composite cylindrical shells under hydrostatic pressure, Ocean Eng. 249 (2022) 110871. https://doi.org/10.1016/j.oceaneng.2022.110871.

[27] S. Zhu, J. Sun, Z. Tong, Q. Li, Z. Zhou, X. Xu, Post-buckling analysis of magneto-electro-elastic composite cylindrical shells subjected to multi-field coupled loadings, Compos. Struct. 270 (2021) 114061. https://doi.org/10.1016/j.compstruct.2021.114061.

[28] W.M. Mahdy, L. Zhao, F. Liu, R. Pian, H. Wang, J. Zhang, Buckling and stress-competitive failure analyses of composite laminated cylindrical shell under axial compression and torsional loads, Compos. Struct. 255 (2021) 112977. https://doi.org/10.1016/j.compstruct.2020.112977.

[29] Y. Zhu, Y. Dai, Q. Ma, W. Tang, Buckling of externally pressurized cylindrical shell: A comparison of theoretical and experimental data, Thin-Walled Struct. 129 (2018) 309–316. https://doi.org/10.1016/j.tws.2018.04.016.

[30] M. Zhang, Y. Yao, H. Pei, J. Zheng, A new isotropic hardening constitutive model based on reference compression curve, Comput. Geotech. 138 (2021) 104337. https://doi.org/10.1016/j.compgeo.2021.104337.

[31] A.R. Prabowo, B. Cao, J.M. Sohn, D.M. Bae, Crashworthiness assessment of thin-walled double bottom tanker: Influences of seabed to structural damage and damage-energy formulae for grounding damage calculations, J. Ocean Eng. Sci. 5 (2020) 387–400. https://doi.org/10.1016/j.joes.2020.03.002.

[32] A.R. Prabowo, R. Ridwan, N. Muhayat, T. Putranto, J.M. Sohn, Tensile analysis and assessment of carbon and alloy steels using fe approach as an idealization of material fractures under collision and grounding, Curved Layer. Struct. 7 (2020) 188–198. https://doi.org/10.1515/cls-2020-0016.

[33] M. Yusvika, A.R. Prabowo, D.D.D.P. Tjahjana, J.M. Sohn, Cavitation prediction of ship propeller based on temperature and fluid properties of water, J. Mar. Sci. Eng. 8 (2020). https://doi.org/10.3390/JMSE8060465.

[34] A.R. Prabowo, T. Muttaqie, J.M. Sohn, B.I.R. Harsritanto, Investigation on structural component behaviours of double bottom arrangement under grounding accidents, Theor. Appl. Mech. Lett. 9 (2019) 50–59. https://doi.org/10.1016/j.taml.2019.01.010.

[35] B.P.P. Caesar, H. Hazimi, H. Sukanto, A.R. Prabowo, Development of novel design and frame structural assessment on mitutoyo's auto checking hardness machine using reverse engineering approach: Series HR-522 hardness tester, J. Eng. Sci. Technol. 15 (2020) 1296–1318.

[36] Cao, B., Bae, D.-M., Sohn, J.-M., Prabowo, A.R., Chen, T.H., & Li, H. (2016). Numerical analysis for damage characteristics caused by ice collision on side structure. Proceedings of the International Conference on Offshore Mechanics and Arctic Engineering - OMAE, 8, V008T07A019. https://doi.org/10.1115/OMAE2016-54727.

[37] A.R. Prabowo, J.H. Byeon, H.J. Cho, J.M. Sohn, D.M. Bae, J.H. Cho, Impact phenomena assessment: Part I-Structural performance of a tanker subjected to ship grounding at the Arctic, MATEC Web Conf. 159 (2018). https://doi.org/10.1051/matecconf/201815902061.

[38] A.R. Prabowo, Q.T. Do, B. Cao, D.M. Bae, Land and marine-based structures subjected to explosion loading: A review on critical transportation and infrastructure, Procedia Struct. Integr. 27 (2020) 77–84. https://doi.org/10.1016/j.prostr.2020.07.011.

[39] D. Mahesa Prabowoputra, S. Hadi, J.M. Sohn, A.R. Prabowo, The effect of multi-stage modification on the performance of Savonius water turbines under the horizontal axis condition, Open Eng. 10 (2020) 793–803. https://doi.org/10.1515/eng-2020-0085.

[40] A.R. Prabowo, T. Tuswan, R. Ridwan, Advanced development of sensors' roles in maritime-based industry and research: From field monitoring to high-risk phenomenon measurement, Appl. Sci. 11 (2021). https://doi.org/10.3390/app11093954.

Paper submitted: 19.06.2022.

Paper accepted: 25.07.2022.